

See discussions, stats, and author profiles for this publication at: <https://www.researchgate.net/publication/231232904>

# Crystallization Behavior of Coordination Polymers. 2. Surface Micro-Morphology and Growth Mechanisms of $[\text{Cu}(\text{bpp})_3\text{Cl}_2] \cdot 2\text{H}_2\text{O}$ by in Situ Atomic Force Microscopy

ARTICLE *in* CRYSTAL GROWTH & DESIGN · DECEMBER 2009

Impact Factor: 4.89 · DOI: 10.1021/cg900987r

---

CITATIONS

8

---

READS

24

## 2 AUTHORS, INCLUDING:



Silvia Rizzato

University of Milan

78 PUBLICATIONS 1,780 CITATIONS

SEE PROFILE

## Crystallization Behavior of Coordination Polymers. 2. Surface Micro-Morphology and Growth Mechanisms of $[\text{Cu}(\text{bpp})_3\text{Cl}_2] \cdot 2\text{H}_2\text{O}$ by In Situ Atomic Force Microscopy

Massimo Moret<sup>\*,‡</sup> and Silvia Rizzato<sup>†</sup>

<sup>‡</sup>Dipartimento di Scienza dei Materiali, Università degli Studi di Milano Bicocca, Via R. Cozzi 53, I-20125 Milano, Italy, and <sup>†</sup>Dipartimento di Chimica Strutturale e Stereochemica Inorganica and Facoltà di Farmacia, Università degli Studi di Milano, Via G. Venezian 21, I-20133 Milano, Italy

Received August 18, 2009

**ABSTRACT:** Crystal growth of the one-dimensional coordination polymer  $[\text{Cu}(1,3\text{-bis}(4\text{-pyridyl})\text{propane})_3\text{Cl}_2] \cdot 2\text{H}_2\text{O}$  was investigated in aqueous solutions by in situ atomic force microscopy. Details about the growth mechanisms of the {001} form at low supersaturation were obtained. In particular, growth hillocks due to simple and complex dislocation sources were observed as the only active mechanism. The thinnest steps observed on {001} faces and delimiting growth hillocks were  $d_{002}$  layers, in accordance with the elementary growth layer expected from the systematic extinction conditions of space group  $I2/a$  and hence from Bravais–Friedel–Donnay–Harker rules and Hartman and Perdok periodic bond chains theory. This feature of the {001} faces suggests that small oligomeric species can be involved in the crystal growth processes. The effects of unknown impurities in the organic ligand upon the growth of crystals of the title compound were also studied.

### Introduction

In recent years coordination polymers emerged from the realm of solid-state structural characterization and topological classification of frameworks<sup>1</sup> becoming of high interest to crystal engineering.<sup>2–4</sup> Recently, they reached full maturity with impressive potential applications in strategic technologies such as gas and solvent recovery.<sup>5–7</sup> In previous work<sup>8,9</sup> about the crystallogenesis of coordination polymers, we discussed the role of kinetics and thermodynamics in the synthesis of a series of  $\text{MCl}_2/\text{bpp}$  polymeric systems ( $\text{bpp} = 1,3\text{-bis}(4\text{-pyridyl})\text{propane}$ ,  $\text{M} = \text{Mn, Fe, Co, Ni, Cu, Cd, Zn}$ ), using solvents such as water, alcohols, dichloromethane, and tetrahydrofuran. These results allowed us to selectively synthesize a variety of metal organic framework species (hereafter MOFs) with different dimensionalities of the coordination networks, coordination sphere at the metal centers, and intertwining of the frameworks. Since the mechanisms that rule formation of this class of compounds are still poorly understood apart from a few cases,<sup>10,11</sup> the rational design of supramolecular coordination networks requires a better understanding of the self-assembling processes involved. This challenge deals, inter alia, with the nature of the solution species and how they assemble into the polymeric networks that we observe in the resulting crystalline solids. In fact, the nucleation step of MOFs is even more intricate than crystal nucleation in “normal” nonpolymeric systems, either inorganic salts or molecular compounds.<sup>12,13</sup>

The last 15 years witnessed the relevant contribution of scanning probe microscopies to the study of crystal growth and dissolution mechanisms at the molecular level, opening new frontiers for validating, refining, and improving accepted theories for crystal growth.<sup>14,15</sup> The ability to perform in situ experiments, thus preserving native conditions for crystal growth, makes atomic force microscopy (AFM) an unmatched tool for investigating crystal growth processes. Up to

now, many systems were successfully studied with this technique, including inorganic salts, minerals, metals, polymers, organic molecules, pharmaceuticals, proteins, and viruses, also including the influence of contaminants or additives.<sup>15,16</sup> As to coordination compounds, there is a large time lag in using AFM compared to other classes of molecules. Few papers reported on metallogrids grown onto inert substrates,<sup>17</sup>  $\text{Co(II)}$  and  $\text{Pd(II)}$  one-dimensional (1D) coordination polymers grown on a graphite substrate,<sup>18</sup> the solvent-mediated transformations occurring during anion exchange in a coordination polymer,<sup>19</sup> and the real time solvent release from a Cu-based MOF associated to anisotropy in mechanical stress caused by the desolvation process.<sup>20</sup> There have been only sparse attempts to improve understanding of the nature of solution species acting as growth units for crystalline MOFs by using the high resolution imaging capabilities of AFM, that is, our preliminary in situ study,<sup>8</sup> recent reports exploiting ex-situ<sup>21,22</sup> and in situ<sup>23</sup> imaging of AFM HKUST-1 crystals,<sup>24</sup> a cubic MOF built upon copper(II) trimesate.

Investigation of MOFs at the microscale is therefore highly relevant for unraveling the mechanisms governing the synthesis of these systems which do really exist only in the solid state, with complex equilibria controlling the distribution of solution species. The need to improve knowledge about crystallographic processes leading to coordination polymers from their basic constituents, that is, metal cations and ligands, prompted us to undertake an in situ AFM study on  $[\text{Cu}(\text{bpp})_3\text{Cl}_2] \cdot 2\text{H}_2\text{O}$  (**1**). We choose this 1D polymeric MOF as a case study due to its monodimensional character which should simplify analysis of results (but see later). The effect of impurities on the growth processes of **1** was also surveyed owing to its relation with crystal morphology and quality of crystals, a primary issue for technological exploitation of MOFs.<sup>25</sup>

### Experimental Procedures

Copper(II) chloride dihydrate (ACS reagent) and 1,3-bis(4-pyridyl)propane (98% purity level) were purchased from Aldrich.

\*Corresponding author: E-mail: massimo.moret@mater.unimib.it.

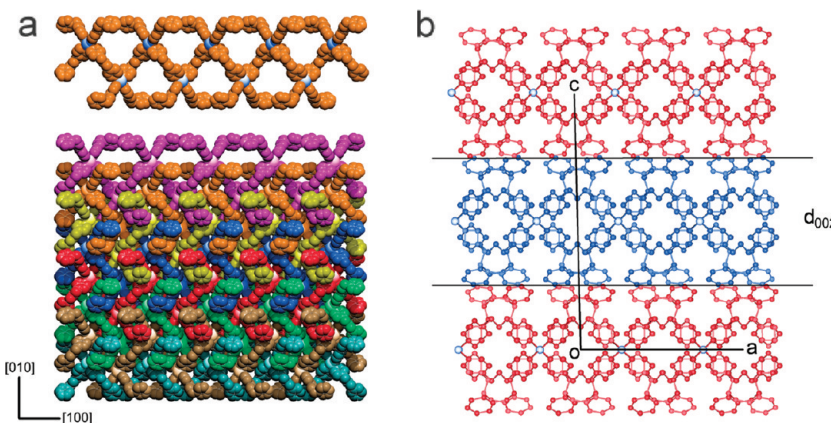


**Figure 1.** (a) Simplified representation of a (001) surface of  $[\text{Cu}(\text{bpp})_3\text{Cl}_2] \cdot 2\text{H}_2\text{O}$  (**1**)<sup>28</sup> with chloride ions, water molecules, and hydrogen atoms omitted for clarity. Polymeric chains are depicted with different colors to enhance the high level of interdigitation of adjacent polymeric chains. Each chain embraces four other chains. At the top of Figure 1a, a single MOF chain shows bidentate bridging bpp ligands defining the zigzag motif and monodentate bpp dangling ligands. (b) View of the structure of **1** along [010] showing the stacking of 2D sheets with thickness  $d_{002}$  and held together by means of  $\pi-\pi$  interactions involving dangling bpp ligands. Water molecules, hydrogen, and chlorine atoms were omitted for clarity.

Bpp ligand was purified by vacuum sublimation. All reactions have been performed in deionized Milli-Q water.  $[\text{Cu}(\text{bpp})_3\text{Cl}_2] \cdot 2\text{H}_2\text{O}$  seed crystals for *in situ* AFM experiments were prepared by spontaneous nucleation from water solutions of  $\text{CuCl}_2$  and bpp in a 1:3 ratio. The solubility curve of **1** has been determined by equilibrating for 3 weeks freshly prepared mixtures of  $\text{CuCl}_2$  and bpp at different temperatures and measuring the equilibrium concentration by solution electroconductance. Solubility resulted in  $S = 1.505 - 0.04167t + 0.00135t^2$  where  $t$  is expressed in °C and  $S$  is in mmol/L in the temperature range 22–40 °C. *In situ* AFM imaging was performed with a Nanoscope IIIa AFM (VEECO) in contact mode with oxide sharpened  $\text{Si}_3\text{N}_4$  or silicon tips of nominal 0.06 or 0.12 N/m force constant. Scan rates were in the range to give 17–60 s per image depending on scan size and surface roughness. All images are unfiltered unless specified. To minimize surface damage, the crystals were quickly transferred from the growth vessel to the AFM fluid cell; the crystal surface was regenerated *in situ* within the AFM cell to reduce possible occurrence of surface artifacts. Supersaturated solutions were fed to the AFM cell (3–5  $\mu\text{L}/\text{s}$ ) with a low noise peristaltic pump (Minipuls 3, Gilson). Experiments were carried out at 22–25 °C. Time series up to 7 h of continuous imaging allowed us to collect growth sequences on the {001} faces of **1**. Force applied to the crystal surface by the AFM tip was minimized to reduce influence of scanning on advancing steps. At the end of each experiment, a larger area was imaged to check for possible erosion phenomena of the surface induced by the scanning process. Differential interference contrast microscopy images were taken with a BX51 Olympus microscope equipped with a Nomarski setup.

## Results and Discussion

Compound **1** was chosen as a model system for *in situ* AFM studies on MOFs to gather information about crystal growth mechanisms and the nature of species that enter the crystal surfaces during accretion of a seed crystal. Important hints about the possible role of secondary building units during crystal growth started to emerge very recently.<sup>21–23,26</sup> Tentative suggestions about possible mechanisms for self-assembling of metal salts and organic ligands leading to MOFs have also been proposed.<sup>27</sup> However, growth of coordination polymers is a highly complex and intriguing process, requiring sound experimental evidence to validate the proposed models. As it will be shown later, even our simple model system **1** poses serious problems when trying to suggest how the solid, containing topologically simple 1D chains, grows from its building blocks. MOF **1** shows zigzag chains made of

octahedral Cu(II) centers, each of them coordinating two bidentate bpp ligands which define the 1D polymeric backbone (Figure 1a, top). Coordination at Cu(II) centers is completed by two trans chloride anions and two dangling monocoordinated bpp ligands. Each of the dangling nitrogen terminals of the monodentate ligands interacts through hydrogen bonding with a water molecule. The zigzag chains develop parallel to [100] and are highly interdigitated along [010] through embracing of dangling bpp ligands (Figure 1a, bottom). Finally, 2D layers of interdigitated chains stack along the *c* crystal axis with  $\pi-\pi$  interactions involving again the uncoordinated pyridyl rings. The 2D interdigitated layers correspond to elementary  $d_{002}$  layers (Figure 1b). This brief summarization of the structural features of **1** is the basis for the subsequent discussion of growth mechanisms observed on the {001} surfaces.

Crystals of **1** several millimeters long can be grown from aqueous solutions<sup>9</sup> with a typical tabular habit [010] elongated as depicted in Figure 2a. The morphologically relevant forms, in order of ascending importance, are {011} (not always present), {010}, {110}, {100}, and {001}. The latter, corresponding to the piling along [001] of 2D sheets of stacked 1D polymer chains, has been observed to be always morphologically dominant and has the lowest grow rate.

Differential interference contrast optical microscopy of {001} faces showed the presence of numerous lens-shaped growth hillocks (Figure 2b), [010] being their major elongation axis due to a significant growth anisotropy. Growth of the {001} faces was studied by *in situ* AFM under low supersaturation  $\beta$  ( $\beta = C/C_{eq}$  with  $C$  and  $C_{eq}$  current and equilibrium molar concentrations, respectively). Apart from intrinsic slowness of AFM imaging limiting the maximum growth rate accessible,<sup>30</sup> higher supersaturations produced explosive 3D nucleation of crystals of **1** and  $[\text{Cu}(\text{bpp})_2\text{Cl}] \cdot 1.5\text{H}_2\text{O}$ <sup>9</sup> within the solution reservoir and the AFM cell due to limited extension of the metastable Ostwald-Myers zone.

At the supersaturation levels used in this study, we never observed 2D nucleation on {001} faces; on the contrary, they grow through a spiral growth mechanism. AFM indeed evidenced the presence of numerous active growth spirals centered at the emerging points of isolated or grouped screw

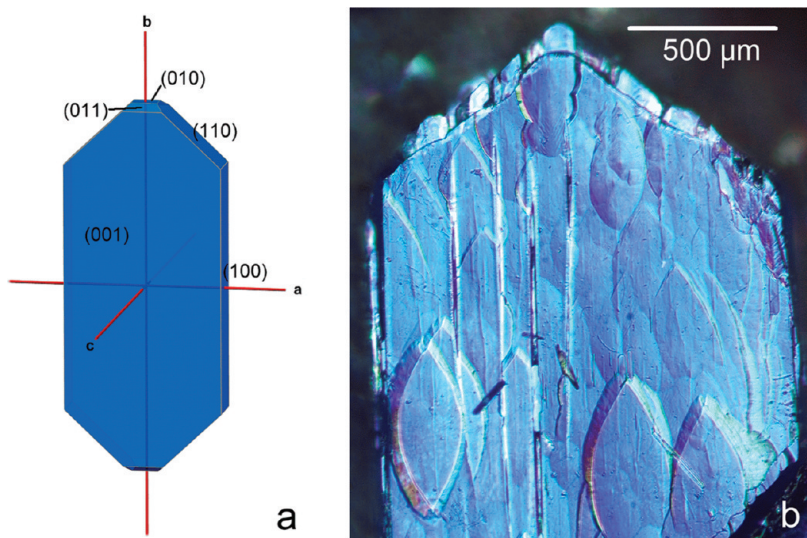


**Figure 2.** (a) Typical growth morphology of crystals of  $\mathbf{1}^{29}$  (b) Differential interference contrast micrograph of a {001} surface after an in situ AFM experiment showing several growth hillocks.

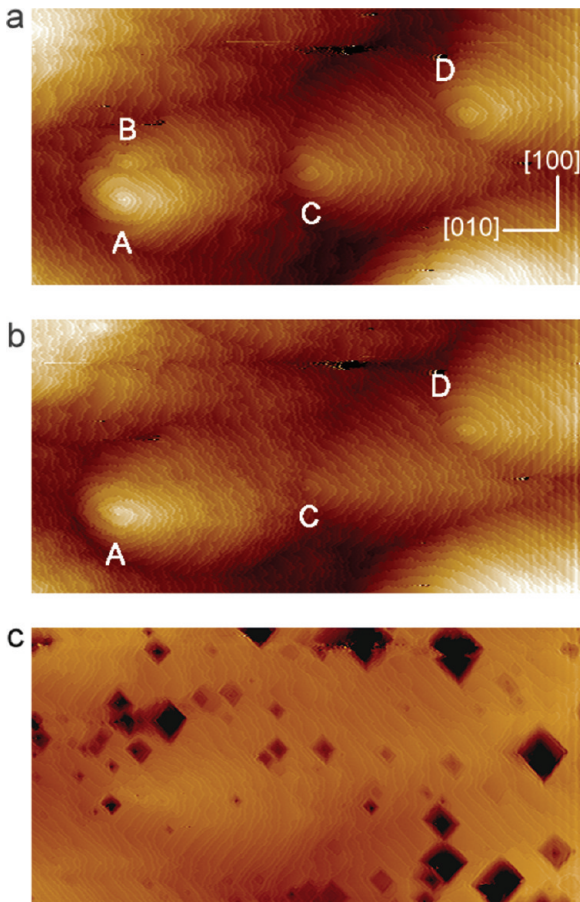


**Figure 3.** AFM image (height mode,  $20 \times 10 \mu\text{m}^2$ ) of a (001) face growing at low supersaturation; (a) growth hillocks pinned at emerging screw dislocations of different strengths. Spiral A has a Burgers vector corresponding to two  $d_{002}$  layers. Spirals B–D emit closed loops due to the presence of pairs of dislocations with an opposite sign at a distance greater than the 2D critical diameter. Single steps are  $14 \pm 0.6 \text{ \AA}$  high, that is, represent elementary  $d_{002}$  layers. (b) The double spiral A submerged the Frank-Read source B. Spiral C is about to be overrun by the stronger spiral A. Image b was taken 14 min after image a. (c) AFM image extracted from a dissolution sequence under a slight undersaturation with etch pits nucleated at the strained cores of screw dislocations.

dislocations (Figures 2b and 3). These growth patterns are typical of flat (F) faces (according to Hartman and Perdok's classification<sup>31</sup>) growing at low supersaturation. The observed spirals were generated either by partial ( $|b| = d_{002}$ ) or multiple ( $|b| = n \times d_{002}$ ) dislocations,  $b$  being the Burgers vector, as could be also observed by etching the crystal surface (Figure 3c).

In Figure 3a, a snapshot from a growth experiment lasting several hours is reported. Within the imaged area (and also beyond its boundaries) the growth activity of the (001) face is ruled only by growth spirals without any evidence of 2D nucleation. The growth hillocks are associated with screw dislocations having different strengths as indicated by the component of the Burgers vector perpendicular to the surface, being  $d_{001}$  and  $d_{002}$  for spirals A and B–D, respectively. Analysis of the growth sequence revealed that spirals B–D of Figure 3 periodically emit closed loops, mimicking birth and spread of 2D nuclei.<sup>32</sup> This indicates the presence of pairs of dislocations with opposite signs and placed at a distance greater than the diameter of the 2D critical nucleus at the chosen supersaturation (see Figure 4g). The three Frank-Read sources B–D and the double spiral A of Figure 3 all have elementary step ledges with a height of  $14 \pm 0.7 \text{ \AA}$  that well compare with the elementary  $d_{002}$  layer spacing of  $13.51 \text{ \AA}$  from diffraction data.<sup>8</sup> Owing to the presence of two elementary steps per turn, spiral A has a greater strength than spirals B–D and its activity overcomes that of adjacent simple spirals. A similar behavior has also been recorded for the protein canavalin.<sup>33</sup> In Figure 3b, taken 14 min after Figure 3a, spiral A has fully overrun source B and is about to overrun also source C by spreading its steps over these weaker sources. Hillock A has slopes of  $0.52^\circ$  and  $0.40^\circ$  along [100] and [010], respectively, while source C has slopes of  $0.30^\circ$  and  $0.24^\circ$  along the same directions. Since lateral advancement of steps emitted by a dislocation source increases the crystal volume, the growth rate normal to the surface is given (in the absence of interactions between the diffusion fields of adjacent steps) by  $R = v \times p$  where  $v$  is the mean lateral speed of steps train and  $p$  is the slope of the growth hillock. Therefore, the higher slope for the double spiral A makes it more effective and in the long run it covers the adjacent simple and less active spirals. These results have been observed several times during different in situ AFM growth experiments.

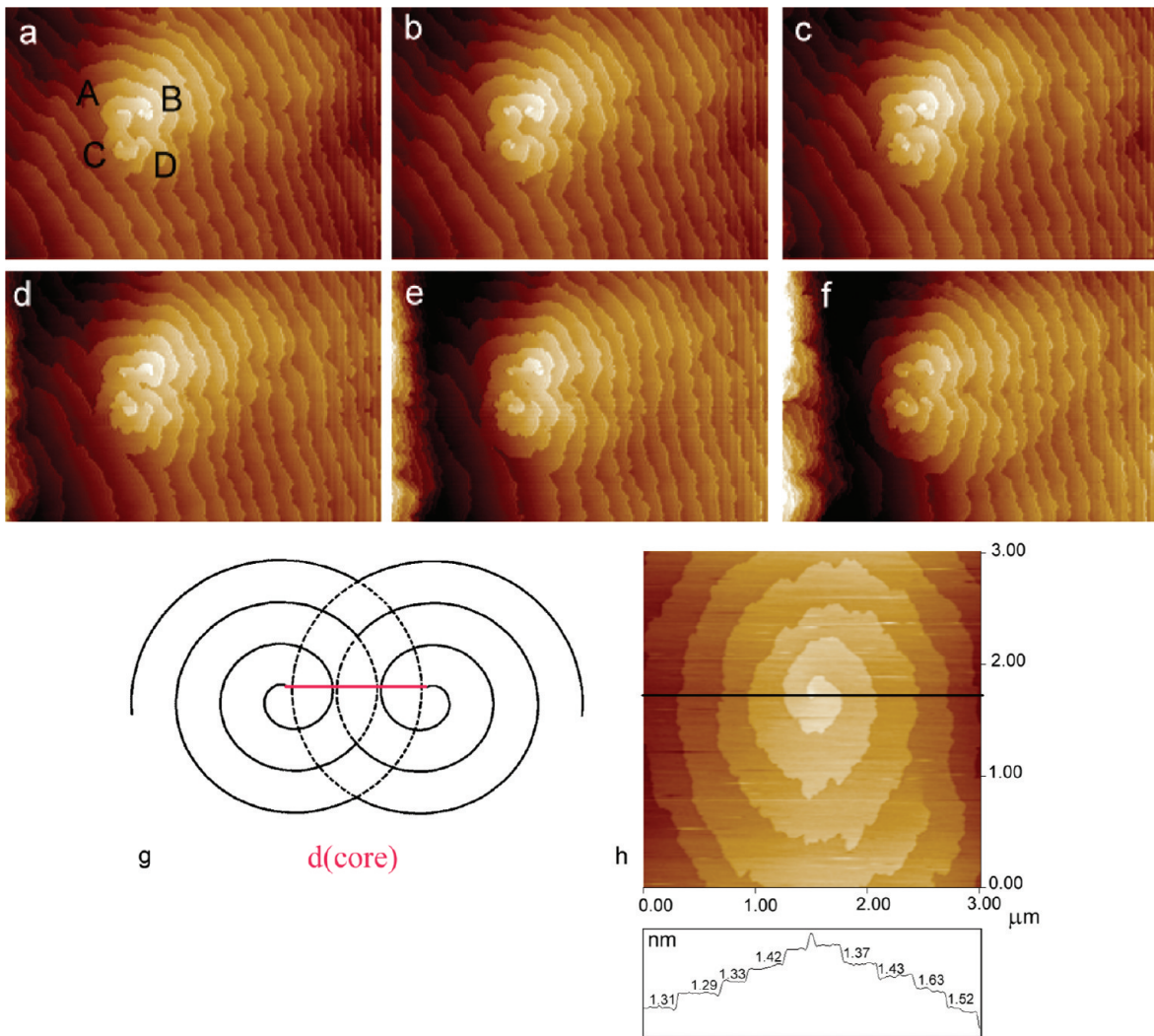


**Figure 4.** (a–f) AFM images ( $7.2 \times 4.8 \mu\text{m}^2$ , height mode; elapsed time between successive images 17 s) of a growing (001) face. Four active screw dislocations emit elementary  $d_{002}$  steps according to their sign. The topmost two are of opposite sign and would emit closed loops if they were not close to the lower dislocation sources. (g) Scheme of two interacting spirals with opposite sign and cores farther apart than the 2D critical nucleus diameter ( $d_{\text{core}} \geq 2r_c$ , Frank-Read source) and periodically emitting closed loops (full line). (h) Cross section profile through a spiral growth showing step height corresponding to elementary  $d_{002}$  layers.

More examples of active growth spirals are shown in Figure 4 where spirals A and D rotate anticlockwise while B and C rotate clockwise. The emitted steps coalesce and/or generate closed loops depending on the rotation phase of spiral arms and the sign of dislocations. Multiple dislocation sources behave depending on their signs and on the ratio between the distance of their cores and the 2D critical diameter  $2r_c$  ( $r_c$  radius of the critical nucleus) at the chosen supersaturation.<sup>32</sup> When the shape of the critical 2D nucleus is circular the spacing between successive steps is  $y_0 = 19r_c$ .<sup>34</sup> Since spacing between successive steps  $y_0$  is inversely proportional to supersaturation, different growth configurations due to interactions between spirals can appear.<sup>32</sup> When the distance between the dislocation cores is greater than the critical length of  $y_0/2$  each dislocation will produce a separate hillock. On the contrary, for a distance less than  $y_0/2$ , steps at the core of the dislocations cannot make a turn about their center and must therefore move around the other dislocation forming a cooperating source. In Figure 4 spirals A and B are close enough to generate closed loops (Figure 4c,d) while spirals C and D, also of opposite sign, work independently from each other with C dominating the activity of D. The steps height

was again  $\sim 14 \text{ \AA}$  indicating the presence of single layers of the polymeric chains during integration of new material into the crystal terraces. This result is relevant for recognizing the nature of the growth units in crystals of MOFs. A similar and noteworthy use of AFM dealt with amino acids for which AFM data suggested that growth units entering steps on the crystal surface comprised dimers of  $\beta$ -alanine and  $\alpha$ -glycine, that is, surface steps advanced by means of bimolecular layers composed of hydrogen-bonded dimers.<sup>35</sup>

Another case of interacting growth spirals is reported in Figure 5. Spirals A and B rotate counterclockwise while C is of opposite sign. These simple spirals work independently producing elementary  $d_{002}$  steps that eventually merge together, perfectly healing the crystal surface. On the contrary, the three defects in the lower third of the scanned area persisted during the whole growth sequence and were filled with mother solution producing micropipes of fluid inclusions.

An example of dislocation sources of even greater complexity is shown in Figure 6 where a grain boundary was imaged. The area comprises about 20 growth spirals, almost all of them with like sign (marked with red arrows in Figure 6). The overall activity due to interactions within the group of spirals

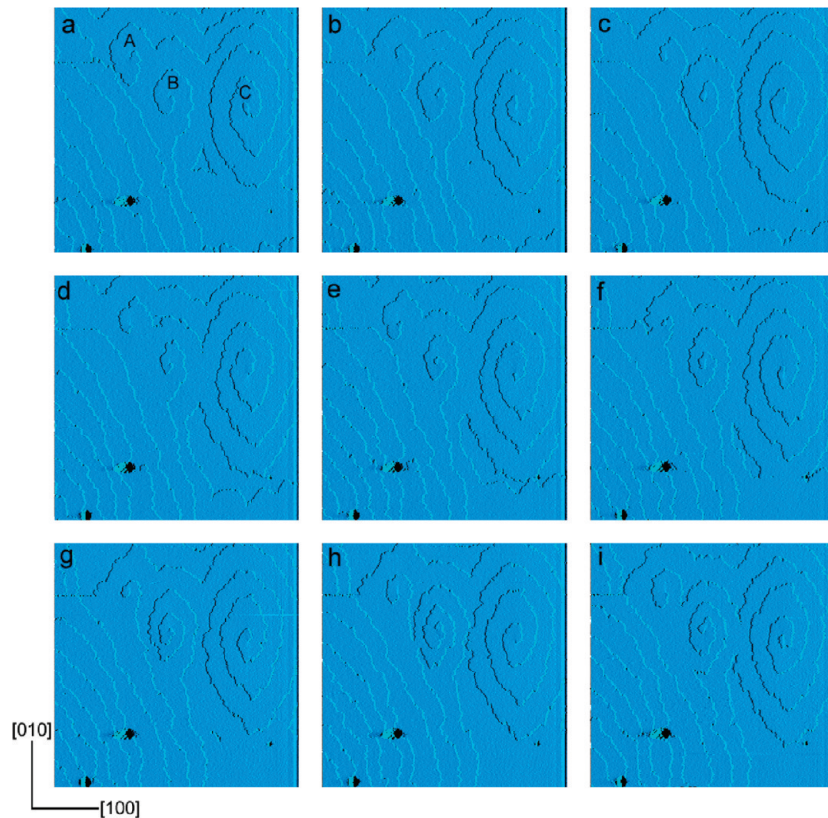


**Figure 5.** AFM sequence ( $6 \times 6 \mu\text{m}^2$ , deflection mode, 46 s interval) of a growing (001) face under a supersaturation  $\beta = 1.05$ . Three simple growth spirals with different signs produce steps that merge together healing the crystal surface. On the contrary the micropipes at the bottom of the scanned area persist and are filled with mother solution.

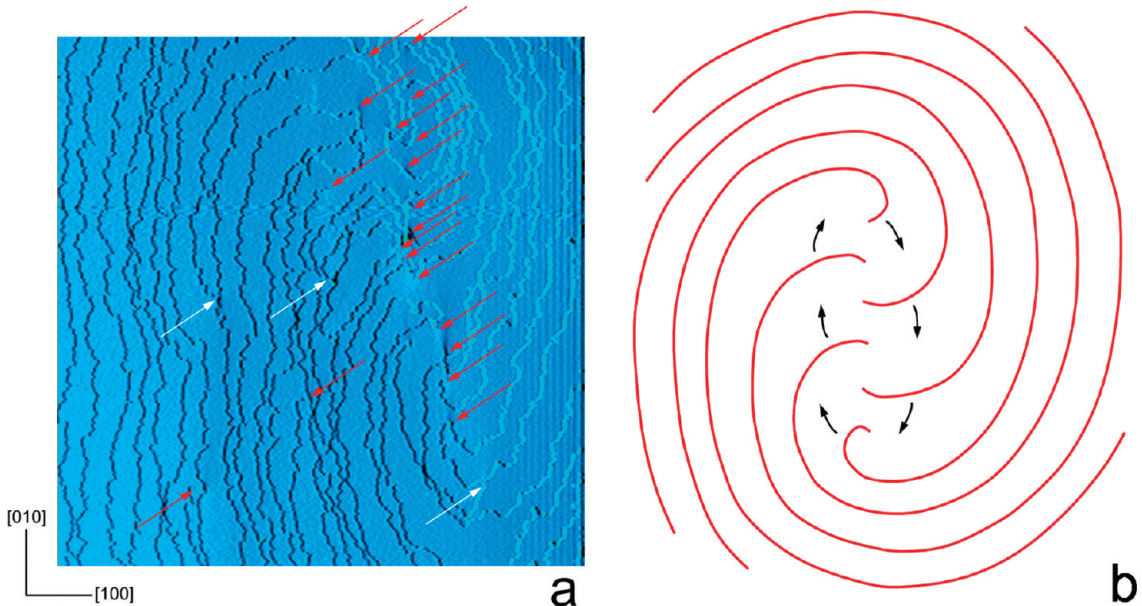


**Figure 6.** (a) AFM image (deflection mode,  $6 \times 6 \mu\text{m}^2$ ) of a growing (001) face under supersaturation  $\beta = 1.05$ . A complex spiral system with several branches is shown. Red and white arrows indicate dislocations of opposite sign. The majority of spirals are lined along a grain boundary and their ensemble rotate around the line of dislocations. (b) Scheme of the activity of a group of dislocations with like sign as expected for a grain boundary.

with like sign is a clockwise rotation of all spiral arms around the line connecting the dislocation cores. This cooperative motion gives great strength to this group of dislocation lines.<sup>32</sup>

Therefore, the growth behavior of **1** compares to observations made for other chemical classes of crystals in recent years by AFM imaging. Our results can be compared to those

recently reported for the 3D MOF HKUST-1 studied ex situ<sup>21</sup> and in situ.<sup>23</sup> For this species ex situ imaging revealed well polygonized growth spirals on {111} faces while in situ AFM provided evidence of birth and spread of 2D nuclei at high supersaturation, and triggering of spiral growth when supersaturation decayed to low levels.

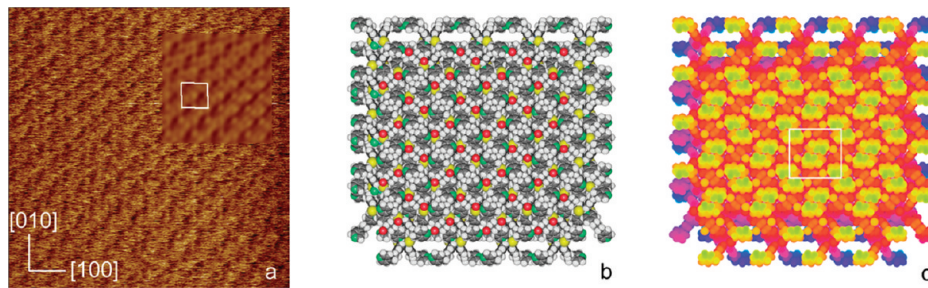


**Figure 7.** (a) Atomic force microscopy image (unfiltered error signal and Fourier filtered inset,  $20 \times 20 \text{ nm}^2$ ) of a growing (001) face under a supersaturation  $\beta = 1.03$ . (b) Model of the bulk terminated (001) surface. Atoms are red O, yellow Cl, green N, blue Cu, white H; (c) simulated AFM model of the (001) surface with the most protruding groups in yellow. The crystal orientation is the same for all pictures.

Particularly interesting is the comparison of growth features observed for {001} faces of **1** with Hartman and Perdock's periodic bond chains (PBC) theory.<sup>31</sup> For many organic and inorganic systems PBC analysis has been very powerful on rationalizing crystal morphologies observed experimentally. According to PBC theory the flat (F), stepped (S), or kinked (K) character of a face is determined by the presence of at least two independent, only one or no PBC vectors, that is, directions of strong intermolecular interactions, within the stoichiometric  $d_{\text{hkl}}$  growth layer. The fact that {001} faces of **1** grow layerwise and are molecularly flat (see Figures 3–7), apart from the cores of screw dislocations, is indicative of their F character in terms of PBC classification. The thinnest steps observed on {001} correspond to single  $d_{002}$  sheets of packed polymeric chains, in agreement with the elementary growth layer expected from the extinction rules of space group  $I2/a$ . Hence, within the elementary  $d_{002}$  layer at least two linearly independent directions must represent strong intermolecular interactions. This experimental evidence is particularly useful to gain insights about the interactions in a complex molecular object such as coordination polymer **1**. A theoretical PBC analysis on compound **1** is presently hampered due the complexity of interactions involving Cu(II) cations, organic and inorganic ligands, and water molecules without suitable potentials to properly model all these species. However, the F character of the {001} form is coherent with the interactions listed when summarizing the main structural features of **1**. Chemical intuition suggests that interdigitation of chains and coordinative bonds along the zigzag polymeric chains should be the most energetically relevant ones. Coordinative bonds are usually assumed to be dominant over other forces (with the exception of strong hydrogen bonds) and therefore should determine the preferred growth direction. In the case of coordination polymer **1** the [100] growth direction should be the fastest one due to its large attachment energy,<sup>36</sup> contrarily to our experimental findings. In other 1D coordination polymers, the idea that coordinative bonds are responsible for the strong growth anisotropy fits better the structural chemist's ability of foreseeing growth anisotropy in crystals,<sup>37</sup> while the present system seems to represent a less clear-cut case. Recent blind tests have shown how difficult predictions of intermolecular interactions and crystal structures are.<sup>38</sup>

Another fundamental information of interest to MOFs designers can be inferred again from the observed height of growing elementary steps, that is,  $d_{002}$ . MOF **1** crystallizes in space group  $I2/a$  and its crystal structure comprises monomolecular layers of interdigitated 1D chains (Figure 1). The recurrent  $d_{002}$  experimental minimum thickness indicates that molecular aggregates present in solution after mixing of

copper chloride and bpp ligand cannot be thicker than one monolayer although possibly oligomeric in nature. The presence of a distribution of oligomeric species could explain the rough profile of steps, although other concomitant physical and chemical effects can be responsible for step roughening, for example, impurities (see later) and unavoidable thermal instabilities during AFM imaging. Molecular level roughness of the growing surfaces allowed us to image for the first time in situ the {001} faces with molecular resolution. It is well-known that in general AFM cannot reach true atomic resolution,<sup>39</sup> however, molecularly resolved images provide details on the surface structure of a crystal, in particular with respect to reconstruction of the bulk.<sup>40</sup> Visualizing the native surface in the presence of the mother solution (Figure 7a) permitted measurement of the lattice periodicity in the (001) plane of  $18.9 \pm 2$  and  $18.5 \pm 2 \text{ \AA}$  along [100] and [010], respectively, with an interaxial angle of  $90 \pm 2^\circ$ . Comparison with *a* and *b* lattice parameters<sup>8</sup> gives for these cell parameters deviations of +10% and +14%, respectively. This discrepancy can be tolerated due to the high thermal drift observed during data acquisition caused by the flowing solution and with only half an hour of thermal stabilization to prevent new steps from crossing the scanned area. Nevertheless, taking into account resolution and accuracy limits of AFM images, the native {001} surface structure is a termination of the bulk structure. Figure 7b reports a structural model built from the X-ray single crystal data.<sup>8</sup> Figure 7c shows a simple steric model<sup>28</sup> emphasizing groups of atoms that should contribute more significantly to the AFM contrast, basically the pairs of dangling bpp ligands protruding out the surface with embracing pyridyl groups. The presence of the *a* glide plane which makes alternating pairs of twisted pyridyl groups mirrored through the *ac* plane is not distinguished by AFM even at molecular resolution, causing the pseudocentered surface *ab* unit cell (Figure 7c) to appear as if centered (Figure 7a).

A final aspect worth mentioning is the action of impurities. In the present case particular emphasis was on possible contaminations arising from the organic bpp ligand. Normally, chemical purity of as-received reactants is high enough to allow synthetic trials of new coordination polymers. However, the presence of foreign molecules in the range of a few % or less within the organic ligand can have detrimental effects on the final outcome of the synthesis reducing the quality of crystals. In recent years, in situ AFM revealed its high potential also regarding the study of the action mechanisms of impurities/additives during crystal growth. Several examples include minerals, inorganic salts, organic molecules, and proteins.<sup>15,16</sup> Unknown impurities imparting a yellow-brown color were always present in the batches of as-received bpp ligand. Concentration of these unknown impurities was

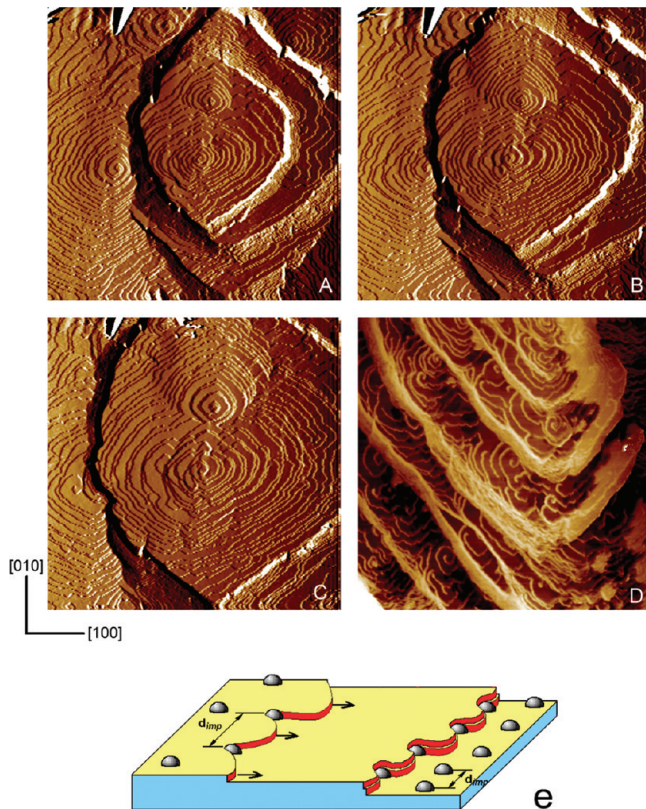


**Figure 8.** (A–D) AFM growth sequence (images a–c  $10.9 \times 10.9 \mu\text{m}^2$ , image d  $15 \times 15 \mu\text{m}^2$ , 28 s interval) of a (001) face in the presence of unknown impurities at supersaturation  $\beta = 1.05$ . (e) Scheme of the Cabrera-Vermilyea model for adsorption of impurities at terraces.

increased by crystallization from ethanol roughly up to 5%. An AFM experiment with use of impure bpp ligand (Figure 8a–c) revealed a striking difference with respect to previous growth sequences where highly purified bpp ligand was employed. The presence of bunched steps as high as 200 nm instead of the monomolecular  $d_{002}$  layers observed under similar supersaturations is shown in Figure 8. This morphological difference can be ascribed to the action of the impurities in the ligand. Also the lateral advancement of steps was clearly disturbed. In Figure 8d heavily bunched steps (20–150 nm) are visible together with bunched steps emitted by dislocation sources whose profiles are strongly distorted by the presence of impurities adsorbed onto the growing surface. As to the action mechanism of foreign molecules different models have been proposed to interpret the kinetics of crystal growth in the presence of additives/impurities.<sup>41</sup> All of them rely on the adsorption of the foreign molecules onto the growing surface. In the case of strong (almost irreversible) adsorption onto the terraces the model of Cabrera and Vermilyea<sup>42</sup> considers immobile impurities distributed on the terraces according to a 2D lattice. When impurities are strongly adsorbed the steps are forced to grow around the impurity molecules (Figure 8e, left). Since steps cannot stay straight when moving through the immobile impurities their reduced radius of curvature decreases their velocity according to the Gibbs–Thomson relation  $v = v_\infty \times (1 - r_c/r)$ , where  $v_\infty$  is the velocity of a straight step,  $r$  is the step curvature, and  $r_c$  is the critical 2D radius at the given supersaturation. Depending on the amount of impurities adsorbed on the surface and therefore their mean separation  $d_{\text{imp}}$  compared to  $r_c$ , lateral

growth is reduced or can even be stopped leading to growth inhibition (Figure 8e, right). Hence, steps can catch up with the first step in the train slowed down or even stopped by the fence of impurities producing a bunch of steps which can be composed of dozens of elementary layers. Adsorption of impurities at kink sites can decrease the integration rate of growth units at steps increasing the average distance between active kinks. This effect produces a stronger polygonization of steps. In our case this morphological effect has not been observed, and on the contrary the steps profile is rounded (Figure 8d). Therefore, it seems plausible a terrace adsorption of impurities possibly akin to the bpp ligand molecules, with a low anisotropy of the direction of adsorption.

## Conclusion

The present paper shows that {001} faces of coordination polymer  $[\text{Cu}(\text{bpp})_3\text{Cl}_2] \cdot 2\text{H}_2\text{O}$  grow at low supersaturation by means of simple and complex growth spirals, while no 2D nucleation was observed. The minimum  $d_{002}$  thickness of growth layers indicates that growth units cannot be of higher thickness but still possibly comprising oligomeric moieties. Growth anisotropy of the {001} spirals does not match the intuitive idea that coordination bonds are stronger than other interactions and thus their direction should be the fastest one during growth. Owing to sparse data about the growth mechanisms of MOFs, the results reported in this study are, in our opinion, a significant improvement for a better understanding of these systems, and of broad interest to crystal engineers of coordination polymers. This aspect is crucial if one thinks that several polymorphic or pseudopolymorphic species are usually obtained under very similar experimental conditions.

**Acknowledgment.** The authors thank Prof. Dino Aquilano (University of Torino) for helpful suggestions about the manuscript.

## References

- (a) Carlucci, L.; Ciani, G.; Proserpio, D. M. *Coord. Chem. Rev.* **2003**, *246*, 247–289. (b) Barnett, S. A.; Champness, N. R. *Coord. Chem. Rev.* **2003**, *246*, 145–168.
- Brammer, L. *Chem. Soc. Rev.* **2004**, *33*, 476–489.
- Soldatov, D. V.; Enright, G. D.; Ripmeester, J. A. *Cryst. Growth Des.* **2004**, *4*, 1185–1194.
- Blake, A. J.; Champness, N. R.; Hubberstey, P.; Li, W.-S.; Withersby, M. A.; Schröder, M. *Coord. Chem. Rev.* **1999**, *183*, 117–138.
- Morris, R. E.; Wheatley, P. S. *Angew. Chem., Int. Ed. Engl.* **2008**, *47*, 4966–4981.
- (a) Llewellyn, P. L.; Bourrelly, S.; Serre, C.; Filinchuk, Y.; Férey, G. *Angew. Chem., Int. Ed. Engl.* **2006**, *45*, 7751–7754. (b) Serre, C.; Mellot-Draznieks, C.; Surblé, S.; Audebrand, N.; Filinchuk, Y.; Férey, G. *Science* **2007**, *315*, 1828–1831.
- Rowell, J. L. C.; Yaghi, O. M. *Angew. Chem., Int. Ed. Engl.* **2005**, *44*, 4670–4679.
- Carlucci, L.; Ciani, G.; Moret, M.; Proserpio, D. M.; Rizzato, S. *Chem. Mater.* **2002**, *14*, 12–16.
- Carlucci, L.; Ciani, G.; García-Ruiz, J. M.; Moret, M.; Proserpio, D. M.; Rizzato, S. *Cryst. Growth Des.* **2009**, doi: 10.1021/cg900985w.
- Levin, M. D.; Stang, P. J. *J. Am. Chem. Soc.* **2000**, *122*, 7428–7429.
- Wheaton, C. A.; Jennings, M. C.; Puddephatt, R. J. *J. Am. Chem. Soc.* **2006**, *128*, 15370–15371.
- (a) Kashchiev, D.; van Rosmalen, G. M. *Cryst. Res. Technol.* **2003**, *38*, 555–574. (b) Davey, R. J.; Allen, K.; Blagden, N.; Cross, W. I.; Lierberman, H. F.; Quayle, M. J.; Righini, S.; Seton, L.; Tiddy, G. J. T. *CrystEngComm* **2002**, *4*, 1–8. (c) Davey, R. J.; Dent, G.; Mughal, R. K.; Parveen, S. *Cryst. Growth Des.* **2006**, *6*, 1788–1796.

- (13) Vehkämäki, H. *Classical Nucleation Theory in Multicomponent Systems*; Springer Verlag: Berlin, 2006.
- (14) (a) Chernov, A. A.; De Yoreo, J. J.; Rashkovich, L. N.; Vekilov, P. G. *MRS Bull.* **2004**, 927–934. (b) Gliko, O.; Reviakine, I.; Vekilov, P. G. *Phys. Rev. Lett.* **2003**, 90, 225503–1/4.
- (15) Ristic, R. I.; De Yoreo, J. J.; Chew, C. M. *Cryst. Growth Des.* **2008**, 8, 1119–1122.
- (16) (a) Gratz, A. J.; Hillner, P. E. *J. Cryst. Growth* **1993**, 129, 789–793. (b) Britt, D. W.; Hlady, V. *Langmuir* **1997**, 13, 1873–1876. (c) Davis, K. J.; Dove, P. M.; De Yoreo, J. J. *Science* **2000**, 290, 1134–1137. (d) Land, T. A.; Martin, T. L.; Potapenko, S.; Palmore, G. T.; De Yoreo, J. J. *Nature* **1999**, 399, 442–445. (e) Mauri, A.; Moret, M. *J. Cryst. Growth* **2000**, 208, 599–614. (f) Li, T.; Morris, K. R.; Park, K. *Pharm. Res.* **2001**, 18, 398–402. (g) Thompson, C.; Davies, M. C.; Roberts, C. J.; Tendler, S. J. B.; Wilkinson, M. J. *Int. J. Pharm.* **2004**, 280, 137–150. (h) Nakada, T.; Sazaki, G.; Miyashita, S.; Durbin, S. D.; Komatsu, H. *J. Cryst. Growth* **1999**, 196, 503–510. (i) Matsuzaki, Y.; Kubota, T.; Liu, X. Y.; Ataka, M.; Takano, K. *J. J. Cryst. Growth* **2002**, 242, 199–208. (j) Plomp, M.; McPherson, A.; Malkin, A. *J. Proteins* **2003**, 50, 486–495. (k) Yoshizaki, I.; Kadokawa, A.; Iimura, Y.; Igarashi, N.; Yoda, S.; Komatsu, H. *J. Synchrotron Radiat.* **2004**, 11, 30–33. (l) Kim, I. W.; Giocondi, J. L.; Orme, C.; Collino, S.; Evans, J. S. *Cryst. Growth Des.* **2008**, 8, 1154–1160.
- (17) Semenov, A.; Spatz, J. P.; Möller, M.; Lehn, J.-M.; Sell, B.; Schubert, D.; Weidl, C. H.; Schubert, U. S. *Angew. Chem., Int. Ed. Engl.* **1999**, 38, 2547–2550surfaces .
- (18) Surin, M.; Samori, P.; Jouaiti, A.; Kyritsakas, N.; Hosseini, M. W. *Angew. Chem., Int. Ed. Engl.* **2007**, 46, 245–249.
- (19) (a) Khlobystov, A. N.; Champness, N. R.; Roberts, C. J.; Tendler, S. J. B.; Thomson, C.; Schröder, M. *CrystEngComm* **2002**, 4, 426–431. (b) Thomson, C.; Champness, N. R.; Khlobystov, A. N.; Roberts, C. J.; Schröder, M.; Tendler, S. J. B.; Wilkinson, M. J. *J. Microscopy* **2004**, 214, 261–271.
- (20) Carlucci, L.; Ciani, G.; Moret, M.; Proserpio, D. M.; Rizzato, S. *Angew. Chem., Int. Ed. Engl.* **2000**, 39, 1506–1510.
- (21) Shöae, M.; Agger, J. R.; Anderson, M. W.; Attfield, M. P. *CrystEngComm* **2008**, 10, 646–648.
- (22) Szelagowska-Kunstman, K.; Cyganik, P.; Goryl, M.; Zacher, D.; Puterova, Z.; Fischer, R. A.; Szymonski, M. *J. Am. Chem. Soc.* **2008**, 130, 14446–14447.
- (23) Shöae, M.; Anderson, M. W.; Attfield, M. P. *Angew. Chem., Int. Ed. Engl.* **2008**, 47, 8525–8528.
- (24) Chiu, S. S. Y.; Lo, S. M. F.; Charmant, J. P. H.; Orpen, A. G.; Williams, I. D. *Science* **1999**, 283, 1148–1150.
- (25) Uemura, T.; Hoshino, Y.; Kitagawa, S.; Yoshida, K.; Isoda, S. *Chem. Mater.* **2006**, 18, 992–995.
- (26) Morris, R. E. *ChemPhysChem* **2009**, 10, 327–329.
- (27) Ramanan, A.; Whittingham, M. S. *Cryst. Growth Des.* **2006**, 6, 2419–2421.
- (28) Keller, E. *SCHAKAL99. A Computer Program for the Graphic Representation of Molecular and Crystallographic Models*; University of Freiburg: Freiburg, Germany, 1999.
- (29) (a) Kaminsky W. *WinXMorph 1.4.9.5. A Program to Draw Crystal Morphologies*; University of Washington: Seattle, WA, USA, 2007. (b) Kaminsky, W. *J. Appl. Crystallogr.* **2005**, 38, 566–567.
- (30) Dove, P. M.; Platt, F. M. *Chem. Geol.* **1996**, 127, 331–338.
- (31) (a) Hartmann, P.; Perdok, G. W. *Acta Crystallogr.* **1955**, 8, 49–52. (b) Hartmann, P.; Perdok, G. W. *Acta Crystallogr.* **1955**, 8, 521–524. (c) Hartmann, P.; Perdok, G. W. *Acta Crystallogr.* **1955**, 8, 525–529.
- (32) Burton, W. K.; Cabrera, N.; Frank, F. C. *Phil. Trans. R. Soc.* **1951**, 243, 299–358.
- (33) (a) Land, T. A.; De Yoreo, J. J.; Lee, J. D. *Surf. Sci.* **1997**, 384, 136–155. (b) Land, T. A.; De Yoreo, J. J. *J. Cryst. Growth* **2000**, 208, 623–637.
- (34) Cabrera, N.; Levine, M. M. *Phil. Mag.* **1956**, 1, 450–458.
- (35) Gidalevitz, D.; Feidenhans'l, R.; Matlis, S.; Smilgies, D.-M.; Christensen, M. J.; Leiserowitz, L. *Angew. Chem., Int. Ed. Engl.* **1997**, 36, 955–959.
- (36) Hartman, P.; Bennema, P. *J. Cryst. Growth* **1980**, 49, 145–156.
- (37) (a) Dinnebier, R.; Lerner, H.-W.; Ding, L.; Shankland, K.; David, W. I. F.; Stephens, P. W.; Wagner, M. Z. *Anorg. Allg. Chem.* **2002**, 628, 310–314. (b) Prokofiev, A. V.; Dahlmann, E.; Ritter, F.; Assmus, W.; Margraf, G.; Wagner, M. *Cryst. Res. Technol.* **2004**, 39, 1014–1019.
- (38) Day, G. M.; Motherwell, W. D. S. *Cryst. Growth Des.* **2006**, 6, 1985–1990.
- (39) Ohnesorge, F.; Binnig, G. *Science* **1993**, 260, 1451–1456.
- (40) Overney, R. M.; Howald, L.; Frommer, J.; Meyer, E.; Brodbeck, D.; Güntherodt, H.-J. *Ultramicroscopy* **1992**, 42–44, 983–988.
- (41) Sangwal, K. *Additives and Crystallization Processes. From Fundamentals to Applications*; Wiley: UK, 2007
- (42) Cabrera, N.; Vermilyea, D. A. In *Growth and Perfection of Crystals*; Doremus R. H., Ed.; Wiley: New York, 1958; p 393.